Variations of Arctic winter ozone from the LIMS Level 3 dataset

Ellis Remsberg[1], Murali Natarajan[1], and Ernest Hilsenrath[2]

[1]Science Directorate, NASA Langley Research Center, 21 Langley Blvd, Mail Stop 401B, Hampton, VA 23681, USA

[2]Fellow at Joint Center for Earth System Technology, University of Maryland at Baltimore County, 1000 Hilltop Circle, Baltimore, MD 21250, USA

Correspondence to: Ellis Remsberg (ellis.e.remsberg@nasa.gov)

(for submission to Atmospheric Measurement Techniques Journal)

~~October, 2021~~January, 2022

Abstract

The Nimbus 7 limb infrared monitor of the stratosphere (LIMS) instrument operated from October 25, 1978, through May 28, 1979. Its Version 6 (V6) profiles and their Level 3 or zonal Fourier coefficient products have been characterized and archived in 2008 and in 2011, respectively. This paper focuses on the value and use of daily ozone maps from Level 3, based on a gridding of its zonal coefficients. We present maps of V6 ozone on pressure surfaces and compare them with several rocket-borne chemiluminescent ozone measurements that extend into the lower mesosphere. ~~Daily,~~We illustrate how the synoptic maps of V6 ozone and temperature ~~illustrate that they~~ are an important aid in interpreting satellite limb-infrared emission versus local measurements, especially when they occur during dynamically active periods of northern hemisphere winter. ~~We then show a~~A map sequence ~~of V6 maps of upper stratospheric ozone,~~ spanning the minor stratospheric warmings of late January and early February ~~1979. The map sequence of V6 geopotential height reveals how ozone was changing in the vortex and~~characterizes the evolution of a low ozone pocket (LOP) at ~~the centers of adjacent anticyclones.~~that time. We also ~~report on zonal variations~~present time series of the wintertime tertiary ozone maximum ~~of the upper mesosphere~~ and its associated ~~temperature fields during winter.~~zonally varying temperatures in the upper mesosphere. These ~~several~~ examples provide ~~a guide~~guidance to researchers for further exploratory analyses of the daily maps of middle atmosphere ozone from LIMS.

1 Introduction and objectives

The historic Nimbus 7 Limb Infrared Monitor of the Stratosphere (LIMS) experiment provided data on middle atmosphere ozone from October 25, 1978, through May 28, 1979, for scientific analysis and for comparisons with atmospheric models (Gille and Russell, 1984). Ozone is an excellent tracer of ~~middle atmosphere~~stratospheric transport ~~processes at~~in the high ~~latitudes~~latitude stratosphere. As an early example, Leovy et al. (1985) showed how daily maps of the LIMS ozone fields correlate well with geopotential height (GPH) fields on the 10-hPa pressure surface. They also reported on the rapidly changing effects of wave activity on ozone, which led to a better understanding of stratospheric transport processes within models.

Hitchman et al. (1989) also analyzed the temperature fields from LIMS and reported on Arctic observations of an elevated stratopause in late autumn to early winter that they associated with momentum forcings from gravity waves.

Current research ~~is focusing~~focuses on the 3-dimensional character of ozone in the upper stratosphere and mesosphere, based on more recent satellite datasets. Several studies ~~report on~~consider how temperature and ozone vary in association with sudden stratospheric warming (SSW) events (Smith et al., 2009; de la Camara et al., 2018; Kim et al., 2020; Shams et al., 2021). Manney et al. (1995) and Harvey et al. (2008) ~~report on~~describe the development of low ozone pockets (LOPs) in the region of the Aleutian anticyclone during winter. Siskind et al. (2005; 2021) ~~report on~~explain the occurrence of a mesospheric cooling associated with SSWs and ~~on~~ the role of gravity waves for modeling ozone in the upper mesosphere~~.~~, respectively. Chandran et al. (2013) ~~developed~~provide a climatology of the Arctic elevated stratopause~~.~~, and Sofieva et al. (2021) ~~analyzed a multiyear dataset~~analyze for regional trends in stratospheric ozone~~ since 2001. LIMS provides similar data on~~. Smith et al. (2011; 2018) report on monthly changes of the tertiary ozone ~~from an earlier decade for further comparisons~~maximum at high latitudes of the upper mesosphere during winter.

The LIMS (Level 2) profiles ~~have been~~were retrieved with an improved Version 6 (V6) algorithm. ~~Those V6 (or Level 2) profiles~~They were archived in 2008 and include ozone, temperature, and GPH that extend from 316 hPa to ~0.01 hPa. ~~The co~~Co-located V6 profiles of water vapor (H_2O), nitric acid vapor (HNO_3), and nitrogen dioxide (NO_2) extend through the stratosphere. Lieberman et al. (2004) analyzed the V6 temperature profiles and found evidence for non-migrating tides in the mesosphere, due to the interaction of the diurnal tide and planetary zonal-wave 1, especially in late January 1979. Holt et al. (2010) analyzed the descent of V6 NO_2 from the lower mesosphere to within the polar stratospheric vortex, where it interacts with ozone. Remsberg et al. (2013) assimilated V6 ozone profiles in a reanalysis model and gained improved estimates of column ozone, especially in Arctic winter. Such reanalysis studies assimilate temperature and ozone profiles within a model framework. However, the models only approximate the effects of small-scale variations, so it is also useful to consider observed variations of the LIMS parameters without resort to a model. Keep in mind that smaller-scale atmospheric variations also contribute to the analyzed intermediate and large-scale fields from V6. This paper ~~provides some examples~~further explores several instances of ~~the~~those larger-scale variations of Arctic ozone, temperature, and GPH.

The SPARC Data Initiative (SPARC-DI) includes monthly zonal averages ~~for~~of V6 ozone up to the ~~chemical species from V6~~0.1-hPa level (see Tegtmeier et al., 2013; SPARC, 2017; and Remsberg et al., 2021). In Section 2 we show January zonal averages of V6 ozone and temperature profiles that extend even higher or to near the mesopause. The V6 Level 3 (map) product provides a 3-dimensional context for those zonal mean data. Daily V6 maps are also an aid in interpretating individual V6 profiles versus correlative data, especially during dynamically disturbed periods. Specifically, in Section 3 we compare several nighttime V6 ozone profiles with those obtained with a rocket-borne chemiluminescent ~~(CHEM)~~ technique (Hilsenrath et al., 1980). Those profile comparisons are for December 15 and for January 27 and 28, when the temperature and ozone fields were affected by planetary wave forcings. There is a corresponding cooling and variations of ozone in the winter lower mesosphere associated with the warming in the upper stratosphere. Section 4 presents variations of ozone and GPH at northern extratropical latitudes during the minor SSW events of late January and early February 1979, as a complement to the more comprehensive findings of Harvey et al. (2008) on the occurrence of LOPs within anticyclones ~~based on~~ determined from satellite solar occultation ~~satellite~~ data. Section 5 ~~gives some details on~~considers the variability of the tertiary ozone maximum in the upper mesosphere during that same period, as an adjunct to ~~the~~ monthly zonal average values reported by Smith et al. (2018). Section 6 ~~considers~~notes that the ~~variability~~maps of V6 ozone ~~within the lowermost extratropical stratosphere~~contain more details about the gradients of atmospheric ozone during disturbed periods, but also cautions users about occasional, pseudo-ozone features in the ~~tropics.~~tropical lowermost stratosphere. Section 7 concludes that the V6 Level 3 product represents an important resource for ~~further~~ studies of the effects of transport and chemistry ~~of middle atmosphere~~on Arctic ozone.

2 Characteristics of V6 Level 3 data

2.1 LIMS measurements and analyses

Nimbus 7 was in a near-polar orbit, and LIMS made measurements at ~1 pm local time along its ascending (A or south-to-north) orbital segments and at ~11 pm on its descending (D or north-to-south) segments. A-D time differences are of the order of 10 hours at most ~~all~~ latitudes because LIMS viewed the atmosphere 146.5° clockwise of the spacecraft velocity vector, as seen from above~~, or 33.5° counterclockwise from its negative velocity vector.~~. The A-D differences narrow from 10 to about 6 hours from 60°N to 80°N, due to the orbital geometry of Nimbus 7. The V6 processing algorithm accounts for low-frequency spacecraft motions that affect the LIMS view of the horizon. As a result, its measured radiance profiles are well registered ~~well~~ in pressure-altitude (Remsberg et al., 2004). Retrieved V6 ozone, temperature, and GPH profiles extend from 316 hPa to ~0.01 hPa and have a vertical point spacing of ~0.88 km with an altitude resolution of ~3.7 km. ~~They occur every ~1.6 degrees of latitude along orbits, and~~Retrieved profile pairs are spaced every 144 km along the orbital track or at every 1.3°, but closer together at the high, turn-around latitudes of the orbital viewing geometry (Remsberg et al., 1990). LIMS made measurements with a duty cycle of about 11 days on and 1 day off over its planned observing lifetime. The LIMS algorithms (Remsberg et al., 2007) do not account for non-local thermodynamic equilibrium (NLTE) effects in ozone (Solomon et al., 1986; Mlynczak and Drayson, 1990) and in CO_2 (Edwards et al., 1996; Manuilova et al., 1998), so there are positive biases in the retrieved V6 ozone throughout the mesosphere during daylight. However, the V6 nighttime ozone is ~~essentially~~more nearly free of NLTE effects below about the 0.05-hPa level~~.~~, except at times of SSWs (see e.g., Funke et al., 2012).

A sequential-estimation (SE) algorithm ~~generated~~was used to generate daily, zonal Fourier coefficients (zonal mean and up to ~~6-wavenumber, sine and~~ six cosine and sine values or 6-zonal wavenumbers) for Level 3 at every 2° of latitude and at up to 28 vertical levels (Remsberg and Lingenfelser, 2010). The V6 SE algorithm uses better estimates of data uncertainty and ~~a shorter relaxation time of ~2.5 days for the~~ its zonal wave coefficients~~, as compared with the earlier~~ have a memory of ~2.5 days, or about half that of the SE algorithm ~~of~~used by Remsberg et al. (1990). The SE analysis is ~~also~~ insensitive to the very few large, unscreened ozone profiles values found in the lower stratosphere, as noted in Remsberg et al. (2013, their Fig. 1a). The SE algorithm combines the coefficients from both the separate A and D orbital segments and effectively interpolates the profile data in time to provide a continuous, 216-day set of daily zonal coefficients versus pressure-altitude ~~for each of the retrieved LIMS parameters. Those combined (A+D) Level 3 coefficients are the basis for a gridding of synoptic maps at 1200Z of ozone and related parameters. Note that Level 3 also contains coefficients from its separate A and D profiles; their 'zonal mean' values correspond to the local time-of-day of their respective measurements. The Level 3 data are in ASCII format for easy access and use.~~ at 1200Z for each of the retrieved LIMS parameters.

2.2 Monthly average V6 data

One can generate monthly average distributions from the daily Level 3 files of temperature, GPH, and species (ozone, H_2O, HNO_3, and NO_2); zonal averages for the V6 species were supplied to ~~the SPARC Data Initiative or~~ SPARC-DI (SPARC, 2017; Hegglin et al., 2021). Tegtmeier et al. (2013) compared the V6 monthly ozone distributions with ones from other satellite-based, limb sensors and reported good agreement throughout the stratosphere. Although the species cross sections ~~of~~for SPARC~~-DI~~ (2017) extend only up to the 0.1-hPa level (~64 km), V6 average ozone extends higher or to about 0.015 hPa (~75 km). Figure 1 shows the latitude-pressure cross section for January from just the descending (D) orbital profiles, which avoids the larger NLTE biases ~~from the~~that affect daytime ozone in the mesosphere. Stratospheric ozone mixing ratios in Fig. 1 have largest values at about 10 hPa near the Equator (> 9.2 ppmv), and they decrease sharply above and below that level. Maximum mixing ratios for the middle to high latitudes occur between 3 to 5 hPa, due to the larger zenith angles and longer paths of the ultraviolet light for production of atmospheric ozone. There is a nighttime ozone minimum of ~1.2 ppmv across most latitudes of the middle mesosphere. A tertiary ozone maximum is present in the upper mesosphere near the winter day/night terminator ~~zones of~~zone in the LIMS measurements for January ~~(~50°S and ~65~~(at about 67°N), in accordance with the interpretation of Marsh et al. (2001). The location (~0.02 hPa) and magnitude (~3.5 ppmv) of the NH maximum ~~agree with~~are somewhat higher and larger than those reported ~~from subsequent satellite studies~~ by Smith et al. (2018, their Fig. 4~~).~~) from more recent satellite datasets. On the other hand, while the V6 ozone poleward of ~~~60~~50°S is also from descending orbital profiles, it corresponds to daylight conditions at the high southern latitudes in January. Thus, the decrease of mesospheric V6 ozone at 0.1 hPa and poleward of ~~60~~50°S in Fig. 1 indicates merely a change from night to day values~~.~~ and agrees with findings of Lopez-Puertas et al. (2018).

Radiances from two 15-μm CO_2 channels are used for retrievals of V6 temperature versus pressure or T(p), and they are ~~also~~ free of NLTE effects below about the 0.05-hPa level (~70 km) (Lopez-Puertas and Taylor, 2001). ~~Retrievals for~~To first order, the V6 T(p) ~~in the stratosphere~~ retrievals account for the effects of horizontal temperature gradients ~~to first order.~~in the stratosphere (Remsberg et al., 2004). Single profile root-sum-squared (or RSS) errors for T(p) ~~range~~vary from 1 K at 10 hPa to ~~greater than ~~~2.5 K in the upper mesosphere~~. Systematic~~, but they do not include possible temperature gradient errors. RSS error from T(p) ~~are~~is the primary source of bias error for ozone, ~~which grow~~growing to ~~of order~~about 16% in the middle mesosphere (Remsberg et al., 2021, Table 1). Random errors become large for single ozone profiles in the upper mesosphere. As a complement to the V6 ozone of Fig. 1, we show the descending (~nighttime) V6 T(p) distribution for January in Figure 2, which extends to near the 0.01-hPa level. The large-scale features of the T(p) distribution compare well with climatological values from the late 1970s (Fleming et al., 1990), having a maximum value of about 285 K at the SH high latitude~~, SH~~ stratopause and minimum values of < 200 K at the tropical tropopause and near the summer mesopause. There is also ~~an apparent~~some elevation of the Arctic zonal-average stratopause.

Figure 3 shows the monthly-average, zonal (wave) standard deviations (SD) about ~~the~~ daily zonal ~~mean~~means of the combined-mode (A+D) V6 ozone for January, where the SD values are ~~also part~~derived from the zonal-wave amplitudes of ~~the LIMS SPARC-DI product~~V6 Level 3. There are relatively small SD values at low latitudes from 7 to 10 hPa; it is assumed that they are a result of ~~both~~smaller-amplitude Kelvin and Rossby-gravity ~~wave activity.~~waves. Effects of more vigorous, planetary wave activity are most apparent at high northern latitudes ~~throughout~~of the stratosphere ~~and~~during winter. Gravity waves also contribute to SD in the ~~upper~~uppermost mesosphere~~.~~ (Siskind et al., 2021). Ozone shows little zonal variation in the SH upper stratosphere of Fig. 3, due to constraints on the upward propagation of planetary waves through the summer zonal easterlies~~.~~ (Andrews et al., 1987). SD values near the tropical tropopause are due mostly to residual effects of emissions from thin cirrus and represent spurious ozone variations (see Section 6).

3. V6 comparisons with rocket-borne chemiluminescent ozone measurements

In this section we consider V6 comparisons with three nighttime, rocket-borne chemiluminescent ozone soundings~~ using the CHEM technique~~ of Hilsenrath (1980)—one at White Sands, NM, (32.4°N, 253.5°E) on December 15, 1978, and two more at Poker Flat, AK, (65.1°N, 212.5°E) on the successive days of January 27 and 28, 1979. ~~Estimated~~The estimated total, rocket ozone error~~ for CHEM ozone~~ is 14% (precision plus accuracy), according to Hilsenrath and Kirschner (1980).

Ozone comparisons for December 15 are in Figure 4~~, where the~~ (top); we plot every other V6 profile and those four ~~V6~~ profiles ~~are spaced about~~ have spacings of 2.6° in latitude~~ along the descending orbital segment with the LIMS instrument viewing in the NNW direction.~~. The short-dashed V6 profile is at 29.2°, and the long-dashed profile is at 37.2°. ~~The location of~~ The solid curve is the V6 profile at 31.8° (at 0611Z) or closest to the rocket ~~ozone~~ sounding ~~lies midway between them.~~from White Sands (at 0541Z). Horizontal bars on the profiles are estimates of ozone error; they overlap between V6 and ~~CHEM~~rocket, except in the upper stratosphere. ~~However, the~~LIMS ozone is larger than rocket ozone in through the upper stratosphere. The corresponding V6 ~~polar~~ ozone map at 4.6 hPa in Fig. 4 (bottom) reveals ~~a region~~an ozone maximum just south of ~~elevated ozone near~~ White Sands (WS—blue dot~~) on that date.~~), along the descending orbital segment of the satellite at (6°N, 265°E—white dot) or viewing in the NNW direction toward White Sands. Note that while zonal variations in the ~~polar plot~~map are from a gridding of the Level 3 coefficients (2° latitude and 5.625° longitude~~) of the Level 3 coefficients,~~), there is no smoothing of the gridded field in the meridional direction; there is good continuity across latitudes, nonetheless. The ~~CHEM~~rocket profile is a local measurement and has a vertical resolution that ranges from 1.5 km at 60 km to 0.1 km at 20 km; the nearby V6 profiles have a lower vertical resolution of ~3.7 km and are an average over the

Formatted: Space Before: 12 pt

finite horizontal length (~300 km or ~3° latitude) of the LIMS tangent layer. There is an ozone maximum along the LIMS view path just to the south of White Sands, which may account for the profile differences. We also note that the ozone field of two days earlier has the region of sharp gradients positioned over White Sands with ozone at only 8 ppmv. Thus, an ozone field that varies in both space and time ~~may~~can lead to ~~a somewhat reduced quality~~additional uncertainties for comparisons ~~between~~of the localized rocket and limb-viewing satellite profiles in Fig. 4.

Because V6 ozone is obtained from retrievals of the measured V6 ozone radiance profiles, the LIMS retrieved temperature profile must be representative of the atmospheric state for the forward model of ozone radiance. Figure 5 (top) shows the corresponding temperature comparisons between V6 and ~~the correlative~~a separate rocket Datasonde instrument~~ (*).~~. Agreement between them is very good throughout the upper stratosphere, ~~which means that the retrieved V6 ozone is nearly unaffected by temperature bias error. Temperatures do not agree as well in the lowermost mesosphere. The map of V6 temperature in Fig. 5 clearly indicates that there are significant variations in the temperature field at 0.68 hPa near 35°N on December 15. Still, there is little evidence of disagreement between V6 and CHEM ozone in Fig. 4 at 0.68 hPa,~~ indicating that the temperature variations are well determined ~~well~~ along the LIMS view path for the forward radiance calculations of V6 ozone and that the retrieved V6 ozone should be nearly unaffected by temperature bias error. The map of V6 temperature (Fig. 5—bottom) shows zonal variations on December 15, although their meridional gradients are relatively weak above White Sands. Conversely, the ozone~~.~~ profiles agree well near 0.68 hPa in Fig. 4, where there are apparent biases between the T(p) profiles. There are significant horizontal gradients near White Sands in the maps of T(p) at 0.68 hPa, but not in ozone (not shown). In fact, the V6 ozone field at that level has a nearly constant value, and ozone is less sensitive (by half) to changes in T(p) at 0.68 hPa than at 4.6 hPa (Remsberg et al., 2007). Co-location is more important for the V6 versus rocket comparisons of T(p) than of ozone in the lower mesosphere.

The two ~~late January~~ comparisons above Poker Flat, AK, occurred at the time of a stratospheric, zonal wave-1 warming event~~ and during a time of advection of air from lower latitudes to near the Pole (~~. Leovy et al~~., 1985).~~. (1985) provide a detailed discussion of the advective changes for ozone in the middle stratosphere during January 1979. Figure 6 (top) shows three ~~co-located~~ V6 ozone profiles from along ~~a nearby descending~~an ascending orbital segment ~~at ~2204Z (nighttime).~~on January 27. The LIMS instrument was viewing from its ~~sub-~~satellite location ~~of~~ (80.~~5~~7°N, ~~130~~113°E) at 2204Z, and the ~~CHEM~~ rocket ozone launch was two hours earlier or at 2005Z at a solar zenith angle of 84° or near the terminator; there is good agreement ~~for ozone~~of the structure between them, even in the mesosphere. A second rocket launch followed at 0833Z of ~~the next day.~~January 28 (Hilsenrath, 1980). Since the separate V6/~~CHEM~~rocket ozone and T(p) comparisons are similar for the two days, ~~we show~~Fig. 6 contains results for January 27 only. The ~~CHEM sonde~~ rocket sounding recorded two ozone maxima, one near 15 hPa and another at about 0.6 hPa ~~and another near 15 hPa, and the V6 profiles of Fig. 6 also have maxima at those levels plus an ozone minimum at about 3 hPa. Agreement is good between the profiles, although the CHEM profile has more vertical structure.~~. The ozone maximum at about 15 hPa is primarily due to advection of ozone of higher mixing ratios from lower latitudes just prior to the warming event. ~~Leovy et al. (1985) provide a more detailed discussion of the advective changes for ozone in the middle stratosphere during January 1979.~~The local maximum at 0.6 hPa was unexpected, based on findings from a larger set of rocket ozone soundings. There is a relative minimum for both V6 and rocket ozone through the upper stratosphere, although V6 ozone is larger. The map of V6 ozone at 4.6 hPa in Fig. 6 (bottom) indicates that the rocket measurement occurs at the center of the minimum, whereas the V6 profiles are averages across it. The ozone profiles in Fig. 6 (top) indicate the relative minimum in a low-ozone pocket (LOP) that extends from about 7 hPa to 2 hPa.

Figure 7 (top) shows the V6 temperature profile comparisons; T(p) from the Datasonde ~~also~~ has more vertical structure, as expected from a localized measurement. ~~Although there is~~ V6 T(p) values reach a maximum of order 250 K at about 3 to 4 hPa. They agree reasonably with the Datasonde values, given that there is significant horizontal structure in the temperature field surrounding Poker Flat~~, the V6~~. The apparent V6 minus Datasonde bias of order 5 K at 3 hPa ought to lead to a V6 minus rocket ozone bias of -40%, according to error estimates for retrieved V6 ozone. However, Fig. 7 (bottom left) indicates that LIMS was viewing Poker Flat across an area of higher temperatures, such that it is likely that there is a spatial mismatch for V6 and

Datasonde T(p) values. The much smaller and positive ozone differences in Fig. 6 support that likelihood. There may also be co-location differences between the rocket temperature profiles agree reasonably with the Datasonde values and indicate that retrieved V6 ozone again has very little bias due to temperature. T(p) values reach a maximum of order 250 K at about 3 to 4 hPa, or where the ozone profiles in Fig. 6 reveal a relative minimum within a low-ozone pocket (LOP) that extends to other levels or from about 7 hPa to 2 hPa.

The polar vortex is located over northern Europe and Asia on January 27; it is shifted off the Pole because of effects from large-scale, planetary waves on the development of SSWs (ozone soundings in this instance. Andrews et al., 1987, Chapter 6). The polar vortex region has low ozone and relatively cold temperatures; stratospheric temperatures over Alaska have a relative maximum (the SSW). The sounding rocket profile from Poker Flat occurs near the center of an anticyclone and in the region of relatively low ozone.

Figure 8 shows that there is concurrent cooling at 0.46 hPa or above the Alaskan anticyclone, and the corresponding nighttime (or D) ozone field exhibits a local maximum at that same level. Conversely, there is a major temperature increase in the Arctic region above the polar stratospheric vortex over northern Europe, where ozone values remain relatively low. Since ozone is an excellent tracer of transport processes in Arctic winter, it can reveal dramatic changes with altitude, associated with this SSW event7 also. In summary, Figs. 4 through 8 show the utility of daily maps from LIMS Level 3 for the validation and interpretation of the ozone fields during dynamically disturbed conditions. In the next section, we consider sequences of polar plots of both GPH and ozone from January 27 through February 17, 1979, to illustrate the value of the V6 Level 3 products for studies of ozone transport over time.

4. Variations of upper stratospheric ozone during stratospheric warmings

Manney et al. (1995) and Harvey et al. (2004, 2008) contain comprehensive analyses about the occurrence of polar anticyclones and their associated LOPs from analyses of GPH and ozone

~~fields from several different satellites. They determined the extent and character of the polar vortex based on meteorological data from the UK Met Office and as obtained from relatively low, vertical resolution radiance profiles from operational, nadir temperature sounders. Those meteorological analyses extend through the stratosphere but only up to the lower mesosphere. The V6 GPH coefficients extend through both the stratosphere and mesosphere, as derived from the V6 T(p) profiles that have a vertical resolution of order 3.7 km. Thus, the LIMS dataset offers potentially more detail about the occurrence of LOPs.~~

~~The first panel of Figure 9~~ shows a map of NH GPH at 4.6 hPa on January 27 for comparison with the ozone map in Fig. ~~6 and the temperature map in Fig. 7.~~6. Lowest ozone values are in the polar vortex, ~~which~~ where the GPH field is asymmetric about the Pole. A second, ~~relatively~~ low value of ozone ~~(or LOP)~~ is associated with the anticyclone over the Alaskan sector. One can determine horizontal winds from gradients of GPH on the 4.6-hPa surface and thereby estimate the transport of ozone to first order. Qualitatively, the direction and strength of the large-scale transport follows from the character of the cyclonic and anticyclonic features on the GPH map. ~~A~~The large-scale cyclonic circulation about the vortex transports air from middle latitudes to across the Pole on January 27. The vortex region has low ozone and is relatively cold, whereas stratospheric temperatures over Alaska show a maximum (the SSW), and the rocket profile above Poker Flat, AK, was near the center of the anticyclone and in the region of relatively low ozone (or LOP).

Ozone is an approximate tracer of transport processes and reveals dramatic changes with altitude associated with this SSW event, even through the winter lower mesosphere. As an example, Figure S1 (in Supplemental Materials) shows a concurrent cooling at 0.46 hPa above the Alaskan anticyclone on January 27, where the co-located ozone field exhibits a local maximum. There is also a major temperature increase above the polar stratospheric vortex over northern Europe at 0.46 hPa, or where ozone values remain low. In summary, Figs. 4 through 7 and S1 indicate the utility of daily maps from LIMS for analyses of the ozone fields during dynamically disturbed conditions.

4. Variation of a low ozone pocket (LOP) from LIMS Level 3

The polar vortex on January 27 was located over northern Europe and Asia; it was centered off the Pole because of effects of large-scale, planetary waves in the development of the SSW (Andrews et al., 1987, Chapter 6). In this section, we show sequences of polar plots of both stratospheric GPH and ozone for February 1979. Manney et al. (1995) and Harvey et al. ~~The other three panels of Figure 9 are a sequence of three daily NH maps of GPH from February 3 to February 17~~(2004, 2008) provide comprehensive analyses about the occurrence of polar anticyclones and their associated LOPs from studies of GPH and ozone fields from several different satellites. They determined the extent and character of the polar vortex based on meteorological data from the UK Met Office or as obtained from relatively low vertical resolution radiance profiles from operational, nadir temperature sounders. The V6 GPH profiles are derived from and have the same vertical resolution as the T(p) profiles. Manney et al. (1995) showed that water vapor is a useful tracer of the meridional transport of air, and the V6 H_2O fields at 6.8 and 10 hPa indicate that low latitude air was transported to the region of the LOP in late January. But the V6 H_2O fields are noisy at 4.6 hPa (not shown). Even so, the V6 Level 3 ozone, T(p), and GPH data offer useful details about the occurrence of LOPs in the upper stratosphere.

Harvey et al. (2004) reported that LOPs occur nominally at about the 5-hPa level. Accordingly, the three panels of Figure 8 show three daily NH maps of V6 GPH from February 3 to February 17 at 4.6 hPa; each successive map is spaced one week from the previous one. This sequence shows that both the vortex and anticyclone weaken during the three weeks following January 27 at this level. The vortex ~~is~~ re-~~centered~~centers on the Pole ~~on~~by February 17, and the anticyclone is nearly absent at ~~this level~~4.6 hPa following the two minor warming events. The map sequence of GPH indicates that there were significant changes in the horizontal transport of ozone in late January/early February. The corresponding three panels of ozone in Figure 9 show the further evolution of ozone, following that of January 27 (in Fig. 6). Even though the anticyclone had weakened during the first week, there was a deepening of the LOP from January 27 to February 3 and a filling of it thereafter.

Was there some chemical loss of ozone from January 27 to February 3 in the region of the LOP? Morris et al. (1998) and Nair et al. (1998) conducted model calculations to show how that could happen. Ozone reactions are affected by changes with latitude of solar insolation, temperature, and loss via NO_x. Nair et al. (1998) reported on the effect of a decrease in the production of ozone for the development of LOPs, as air parcels in the middle stratosphere move from low to high latitudes or to higher solar zenith angles in winter. Remsberg et al. (2018) analyzed air parcel trajectories that included chemistry, and they showed that there was some loss of ozone in the middle stratosphere, due to reactions with NO_x. However, Holt et al. (2012) analyzed V6 NO_2 in the winter polar vortex, and they did not find enhanced values at 4.6 hPa due to energetic particle precipitation (EPP) by late January.

Figure 10 (left) is a map of the V6 descending orbital (nighttime) NO_2 for January 27 at 4.6 hPa. Based on the corresponding map of GPH in Fig. 7, one can trace the horizontal advection of high NO_2 toward higher latitudes and toward the polar vortex as well as the advection of low NO_2 out of the vortex and about the anticyclone. Fig. The map sequence in Fig. 9 also indicates that there are significant changes in the horizontal transport of ozone during this dynamically active period.10 (right) is a map of HNO_3 at 4.6 hPa. It has a weak, relative maximum above the anticyclone that appears as a residual from the advection of much higher vortex values from several days before. A closer inspection in time reveals that the NO_2 values in the LOP were a bit lower by January 31, when ozone had already declined to near its February 3 value. Thus, while an excess of HNO_3 in the region of the LOP is consistent with a conversion of NO_2 to HNO_3 above the isolated anticyclone, there is no clear evidence from the V6 map products that such chemistry led to significant changes in the ozone. One must conduct trajectory studies that include chemistry and that rely on the V6 species profiles as input for better, quantitative estimates. Unfortunately, the profiles of V6 NO_2 and HNO_3 become noisy in the upper stratosphere. At a minimum though, one can follow the evolution of the LOP using the daily maps of V6 ozone and GPH. Morris et al. (1998) conducted model calculations to show that there can be chemical changes of ozone in the upper stratosphere at that time. Ozone reactions are affected by changes with latitude in solar insolation, temperature, and NO_x. As an example,

Figure 10 (top left) is a map of the V6 descending (nighttime) NO_2 on January 27, and it shows that air having larger NO_2 values was transported northward from middle latitudes toward the anticyclone. Thus, it is likely that there is some loss of ozone due to reactions with NO_x (and NO_2) in the middle stratosphere that is contributing to the LOP feature. The other three panels of Figure 10 show the evolution of ozone for February 3 through 17, following that of January 27 (in Fig. 6). Based on the GPH panels of Fig. 9, there was a deepening of the LOP from January 27 to February 3, but a filling of it thereafter. Transport of air from middle to higher latitudes decreased from February 3 to February 17, when the vortex and anticyclone weakened. But the anticyclone also weakened from January 27 to February 3. Thus, a chemical loss of ozone due to NO_x may also have occurred during that first week. Although we do not show a sequence of maps for other levels, the V6 Level 3 product indicates significant variations in ozone, temperature, GPH, and NO_2 throughout the upper stratosphere.

5. Variations of the tertiary ozone maximum

Smith et al. (2018) describe the changing monthly, zonally averaged character of the wintertime tertiary ozone maximum of the polar upper mesosphere. They point out that the low latitude edge of the tertiary ozone maximum is where HO_x radicals and the chemical loss of ozone due to reactions with them are reduced. The Level 3 ozone and temperature products provide daily, 3-dimensional information about those processes. The top two panels of Figure 11 are of upper mesospheric ozone on the 0.022-hPa surface (~72 km) for January 13 and February 10, respectively. The bottom two panels show the variations of temperature on those same days. First, consider the two ozone plots, which are from only the descending (or nighttime) orbital segments. V6 ozone radiance profiles have low signal-to-noise in the upper mesosphere; the precision estimate for retrieved ozone and its Fourier coefficients is 0.32 ppmv at 0.022 hPa. Therefore, we show gridded ozone maps in Fig. 11 based on just the zonal mean and the sine and cosine coefficients for waves 1 and 2. Elevated values of ozone occur at a lower latitude on January 13 than on February 10, which is consistent with the slightly different location of the terminator on those two days. One can also see that the tertiary maximum has a larger value on February 10 than on January 13is 0.32 ppmv for retrieved ozone profiles. We show a map in Figure 11 of the combined V6 ozone for December 15 at 0.022 hPa (~72 km), where its distribution in the subpolar region is based on fewer than 13 zonal coefficients because some profiles do not extend to that pressure altitude. The corresponding map of temperature is also in Fig. 11, and one can see that there is significant non-zonal structure in its field at the latitudes where ozone is enhanced. While both V6 ozone and temperature are not highly accurate due to NLTE effects in the upper mesosphere, their maps reveal significant relative spatial structures indicating advective transport and its likely effects on ozone.

~~The bottom two~~ Figures S2 and S3 in the Supplemental Materials show additional panels at 0.022 hPa of ~~Fig. 11 are maps of~~ ozone and temperature, respectively, for January 13 ~~and~~, February 10, ~~respectively, for comparison~~and March 1. Elevated values of ozone occur at higher latitudes on February 10 and March 1 than on December 15 and January 13, which is consistent with the ~~ozone fields.~~more northward position of the terminator away from winter solstice and the consequent effects for the chemical loss of ozone. The temperature ~~maps~~ fields are also perturbed on January 13 and February 10, but they are ~~gridded from the zonal mean and coefficients out to zonal wavenumber 6. There is significant zonal structure in them, and temperatures are much warmer in the Canadian sector on January 13 than on February 10. There are~~ more nearly zonal by March 1. However, there are meridional gradients of temperature on ~~both~~all three days~~.~~ in the region of the tertiary ozone maximum. On January 13 there is also a well-defined mesospheric vortex in GPH (not shown), and the highest values of ozone correlate reasonably with it~~; by February 10 the vortex was disturbed at this~~. The vortex is most disturbed and tertiary ozone maximum has largest values on February 10, perhaps in response to the upward propagation of wave activity following the minor SSW of late January.

Figure 12 shows time series of peak zonal mean ozone at 0.022 hPa and its latitude location for each week from November through mid-March. The separate time series are for peak ozone (bottom two series) and their latitude locations (top two). Dashed red curves represent zonal mean results for combined (A+D) ozone; solid black curves are results for nighttime (D) only. Blue horizontal lines represent the approximate latitude position of the terminator. Peak nighttime ozone values are based on just the 'zonal mean' and the cosine and sine coefficients for waves 1 and 2 because not all profiles reach to the 0.022-hPa level. ~~Recall that~~Peak ozone occurs at lower latitudes (~65°N) in December, increasing to ~75°N in early November and early February and to near 80°N by early March. The latitude time series of peak ozone values is reasonably coincident with the changing location of the terminator. Peak combined (A+D) ozone increases slowly from a minimum of 2.2 ppmv in November to 3.6 ppmv in late February and March. Descending (or nighttime only) ozone varies from 3.3 ppmv in November, to ~4.5 ppmv in January, to a maximum of 6.3 ppmv in mid-February, and then declining to 3.5 ppmv by mid-March, although the time series shows rather large variations. Those maximum V6 values are larger than reported by Lopez-Puertas et al. (2018), perhaps due to biases from V6 T(p) and/or ozone at 0.022 hPa.

The increasing V6 ozone in Fig. 12 during winter disagrees with that of Smith et al. (2018), who found decreasing ozone in February. They reported that, in most years, there is a slow descent of relatively dry air into the vortex region in late autumn and early winter in the upper mesosphere, and that the reduction in water vapor implies that there are fewer HO_x radicals for the destruction of ozone near the terminator zone, leading to accumulations of ozone. However, there were two minor warmings and associated lower mesospheric cooling events during late January and early February~~.~~ 1979 (Hitchman et al., 1989). The enhanced V6 ozone of February 1979 follows those SSW events. It ~~is very likely~~may be that there were wave-driven disturbances ~~in the upper mesosphere during that time, due to filtering of gravity waves and their~~ and a dissipation of their energy in the upper mesosphere at higher latitudes at that time (e.g., Siskind et al. 2005). ~~We infer that the warmer temperatures of mid-January at this level led to a radiative relaxation and a descent of relatively dry air into the vortex region. A reduction in water vapor will mean that there are fewer HO_x radicals for the destruction of ozone near the terminator zone, leading to an accumulation of ozone by February 10. Although the seasonal~~One should be able to gain more information about the evolution of the tertiary ozone maximum ~~is understood reasonably well (Smith et al., 2018), there is more information about this ozone feature~~in the winter of 1978-79 from the daily maps of V6 ozone, T(p), and GPH ~~from Level 3.~~(as in Figs. S2 and S3).

6. Other aspects of V6 Level 3 ozone ~~in~~

The combined (A+D) Level 3 coefficients are the ~~**lowermost stratosphere**~~basis for a gridding of daily synoptic maps at 1200Z of ozone and related parameters. The Level 3 product also contains coefficients from its separate A and D profiles; their 'zonal mean' values correspond to the local time-of-day of their respective measurements. Remsberg et al. (2007) noted that maps from V6 reveal more details about the variations of ozone. In Figure S4 of the Supplemental Material we compare a map of V6 ozone at 10 hPa on 27 January with a similar map for V5 of Leovy et al. (1985). The ozone gradients are more pronounced with V6 than with V5 at both the subtropical and vertex edges of the ozone field. The V6 maps make use of all profiles along the orbit, and the SE mapping algorithm was applied to them every 2° of latitude. However, the tighter gradients were also achieved with the V6 algorithm because it has a relaxation time (or memory) that is half that of V5. This means that the V6 maps are more representative of the rapidly changing atmospheric ozone fields on that day. Similar version differences are evident throughout winter, when the so-called 'stratospheric surf zone' develops and expands (Leovy et al., 1985).

~~**6.**~~

Significant exchanges of air and ozone occur from the extratropical stratosphere to the troposphere in winter and spring (Gettelman et al., 2011). ~~Figure 3 also showed that there~~There are large zonal variations about the daily zonal means of ozone in the Arctic region of the lower stratosphere in Fig. 3. There are similar variations in GPH (and derived winds) and in zonal wave activity that lead to ozone transport. Zonal variations are resolved in the daily ozone maps down to the 146-hPa level. ~~In fact~~Notably, Shepherd et al. (2014) integrated the V6 monthly zonal mean ozone above the tropopause and subtracted it from observed total ozone, as part of their assessment of long-term trends of tropospheric ozone from models. Their ~~calculation~~determination of extratropical tropospheric ozone based on LIMS agrees with that obtained from other ozone datasets.

There is also a relative excess of SD ozone values in Fig. 3 centered at 68 hPa at tropical latitudes, and similar anomalies occur in other LIMS months~~, too~~ (not shown). As an example, Figure ~~12~~13 shows ~~an~~a map of V6 ozone ~~map~~ at 68 hPa (~18 km) ~~for the correlative measurement day of~~ on December 15~~, 1978~~, to give more insight about the source of the tropical

Formatted: Font: Not Bold

Formatted: Font: Not Bold

Formatted: Normal, No bullets or numbering variations. Ozone mixing ratio values in Fig. ~~12~~13 are of order 2 to 3 ppmv at high latitudes, becoming much smaller in the subtropics. However, there is also an unexpected, high value of 2 to 3 ppmv at about 15°N, 150°E. Limb measurements in the ozone channel include radiance effects from cirrus particles that can occur along the tangent view path, although the retrieved ozone mixing ratio profiles were screened of those effects to first order (Remsberg et al., 2007). Even so, we note that ozone is easily affected by any excess radiance because of highly non-linear effects for retrievals of ozone ~~from the radiances~~ in the lower stratosphere. It is very likely that the anomalous ozone at 68 hPa is a result of residual effects from subvisible cirrus, which is nearly ubiquitous over the western tropical Pacific region (see SPARC, 2006, Fig. 1.8).

While individual V6 ozone profiles may include such spurious features in the tropics, the Level 3 ozone product at 68 hPa is affected mainly when there is an organized convection and outflow of air that ~~persist~~persists for several days. The adjacent map of ~~tropical~~ ozone at 46 hPa appears unperturbed in that region (not shown), and tropical ozone at 100 hPa approaches zero. There are much smaller anomalies in maps of nitric acid, as its mixing ratio retrieval is very nearly linear. Anomalies are also not ~~present~~so apparent in maps of V6 H_2O at 68 hPa because the cloud screening algorithm for H_2O accounts for the larger vertical field-of-view and extent ~~over~~in altitude for ~~the~~ measurements ~~of~~in the water vapor channel of LIMS. To summarize, one must be mindful that the Level 3 product may ~~show pseudo~~indicate excess, but spurious ozone at 68 hPa in the tropics~~, but likely not in the extratropics~~.

7. Conclusions ~~on the utility of LIMS V6 Level 3 ozone~~

This report provides guidance to researchers for their use of the LIMS V6 Level 3 product and for their generation of daily gridded distributions of its temperature, ozone, and GPH on pressure surfaces. H_2O, NO_2, and HNO_3 are also available for the stratosphere from the Level 3 product. The V6 dataset represents an early baseline for considering possible changes in the middle atmosphere from 1979 to today and into the future. ~~Atmospheric concentrations of the greenhouse gases (GHG), CO_2, CH_4, and CFCs, were smaller in 1979 versus now. As an example, the LIMS algorithm for retrieving T(p) profiles is based on a middle stratosphere CO_2~~

value of 327 ppmv, compared with ~415 ppmv in 2021. As a result, middle atmosphere T(p) distributions were warmer in 1979, which affects both the chemistry and transport of ozone. LIMS alsoLIMS made measurements at a time when stratospheric effects from volcanoes were minimal and when catalytic effects of chlorine on ozone were relatively small. Accordingly, Stolarski et al. (2012) found small, but significant changes in the distribution of upper stratospheric ozone for recent decades compared with 1978-1979. The LIMS measurements were taken near solar maximum and when atmospheric concentrations of the greenhouse gases (GHG), CO_2, CH_4, and CFCs, were smaller than today. Middle atmosphere T(p) distributions were warmer in 1978-1979.

The LIMS measurements in the winter Arctic region occurred when there was a lot of wave activity for the transport and mixing of ozone. Ozone variesAs a result, ozone varied dramatically in winter, particularly during times of stratospheric warming events. There was a so-called Canadian warming in early December 1978, two minor SSW events in late January and early February, and a final warming in late February 1979. We showed V6 comparisons with temperature and ozone profile data obtained using rocket- borne Datasonde and chemiluminescent (CHEM) techniquesinstruments, and we pointed out how an examination of changes in their nearby fields are essentialis valuable for the interpretation and validation of V6 profiles against those correlative measurements. The Level 3 dataset provides daily details on those variations inof ozone with latitude, longitude, and altitude, along with related variations in temperature, geopotential height, NO_2, and $NO_2$$HNO_3$. We noted also that there are instances of spurious, excess ozone from the Level 3 coefficients at 68 hPa in the tropics but not in the extratropical stratosphere. One may find that there are regional changes in ozone in recent decades compared with that in 1978-1979 from V6 (see, e.g., Sofieva et al., 2021).

We displayed evidence of a low ozone pocket (LOP) during the minor SSW of late January above the Aleutian anticyclone, and we followed its evolution into mid-February. The V6 nighttime ozone is accurate up through the middle mesosphere, and surface maps of the large-scale variations of ozone are relatively accurate through the upper mesosphere. Daily ozone and temperature maps reveal zonal wave featuresmesosphere in the regionArctic winter. We provided time series of the wintertime, tertiary ozone maximum of the upper mesosphere~~.~~ from V6 data. Its ozone reached maximum values in February, perhaps as a response to enhanced wave activity in the mesosphere following several SSW events. Together with V6 maps of T(p) and GPH, one may explore further the daily evolution of that ozone maximum throughout the NH winter of 1978-1979.

Data Availability

The LIMS V6 Level 3 product is at the NASA EARTHDATA site of EOSDIS and its website: https://disc.gsfc.nasa.gov/datacollection/LIMSN7L3_006.html (Remsberg et al., 2011). The SPARC-Data Initiative data are located at https://doi.org/10.5281/zenodo.4265393 (Hegglin et al., 2021). We acknowledge the individual instrument teams and respective space agencies for making their measurements available, and the Data Initiative of WCRP's (World Climate Research Programme) SPARC (Stratospheric Processes and their Role in Climate) project for organizing and coordinating the compilation of the chemical trace gas datasets used in this work.

Author Contributions. ER wrote the manuscript and prepared the figures with contributions from his co-authors. EH provided his rocketsonde data on ozone and temperature along with their error estimates.

Competing interests. The authors declare no competing interests for this study.

Acknowledgements. The authors appreciate John Gille and Jim Russell III and members of the LIMS Science Team for their leadership in the development of the LIMS instrument and ~~on the~~for their processing of its historic data products. The authors are grateful to John Burton, Praful Bhatt, Larry Gordley, B. Thomas Marshall, and R. E. Thompson for producing the V6 Level 2 dataset. They acknowledge Gretchen Lingenfelser for her work in generating and archiving the V6 Level 3 coefficient dataset. They appreciate especially the constructive comments from the two anonymous referees. They also thank V. Lynn Harvey for her comments on ~~a~~an early draft~~ version~~ of the manuscript. EER and MN carried out their work while serving as Distinguished Research Associates of the Science Directorate at NASA Langley.

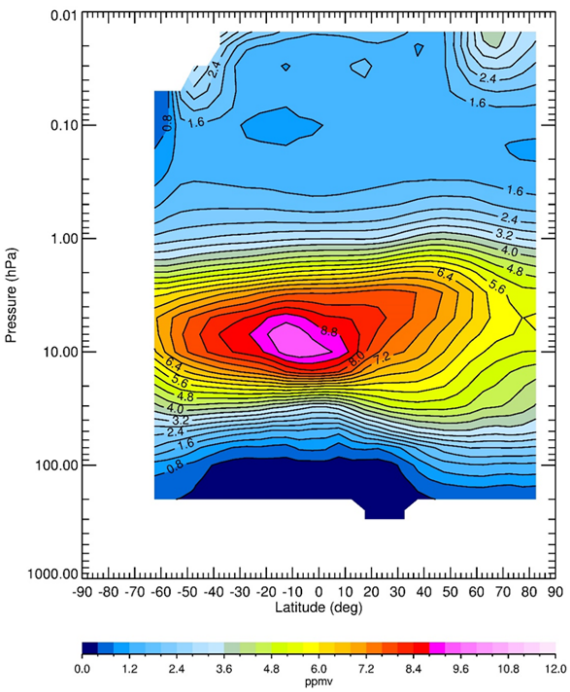

Figure 1—LIMS V6 Level 3 monthly zonal mean ozone for descending-mode only (or nighttime equatorward of ~55°S) for January 1979. Contour interval (CI) is 0.4 ppmv.

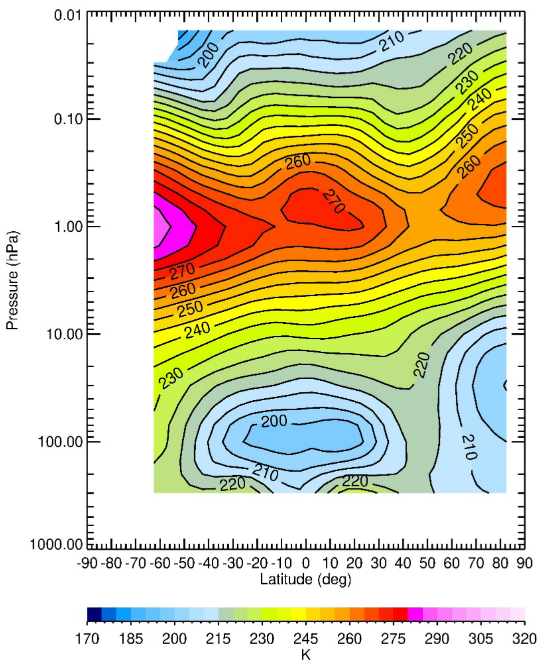

Figure 2—Zonal average, descending-mode, temperature for January 1979. CI is 5 K.

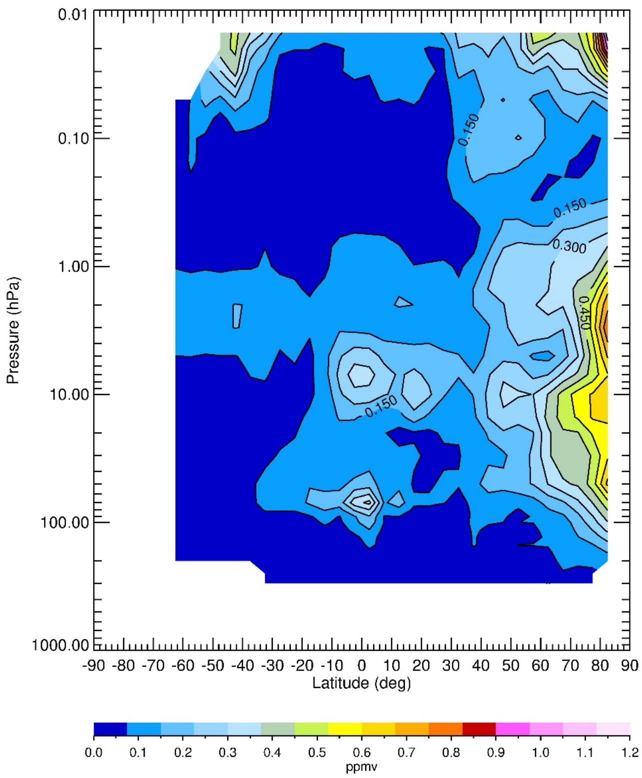
0.01
0.10
1.00
10.00
100.00
1000.00
Pressure (hPa)
-90 -80 -70 -60 -50 -40 -30 -20 -10 0 10 20 30 40 50 60 70 80 90
Latitude (deg)
0.150
0.150
0.300
0.450
0.150
0.0 0.1 0.2 0.3 0.4 0.5 0.6 0.7 0.8 0.9 1.0 1.1 1.2
ppmv

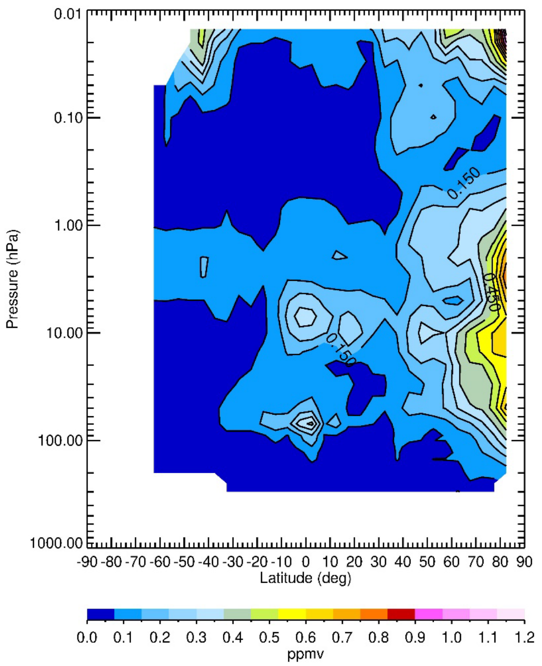

Figure 3—Zonal standard deviation about ~~the~~ average ~~of~~ (A+D) zonal mean ozone for January 1979. ~~Contour interval~~CI is 0.075 ppmv.

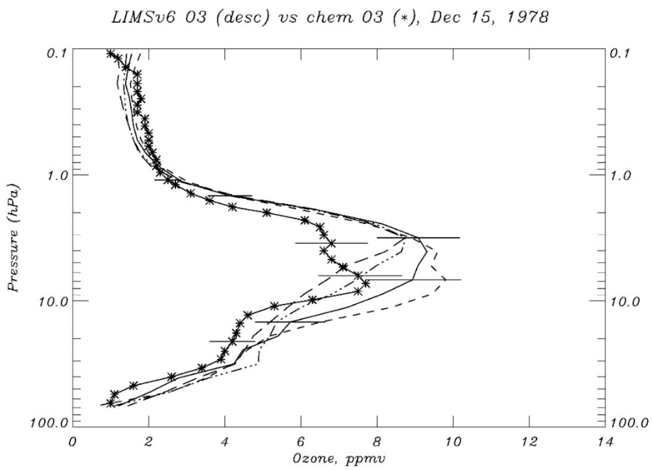
LIMSv6 O3 (desc) vs chem O3 (*), Dec 15, 1978
Pressure (hPa)
0.1
1.0
10.0
100.0
0
2
4
6
8
10
12
14
Ozone, ppmv

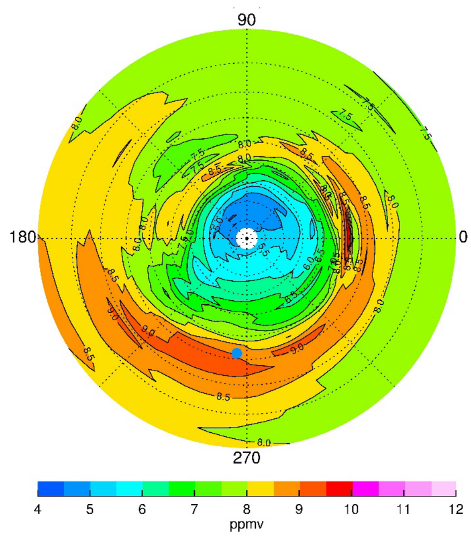
90
180
0
270
4
5
6
7
8
9
10
11
12
ppmv

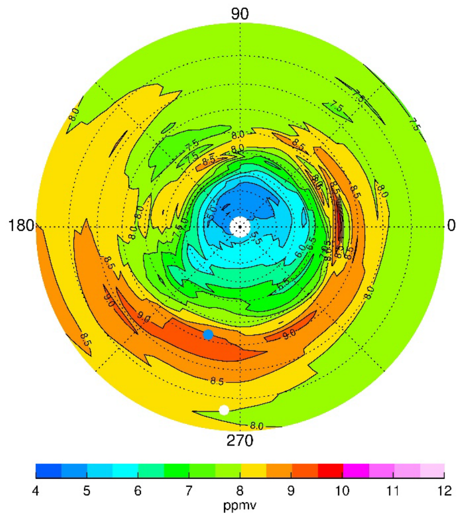

Figure 4~~—~~(top) Profiles of V6 ozone ~~compared with CHEM sonde~~(at 0611Z) versus rocket chem ozone ~~(*)~~(* at 0541Z) on December 15. The four V6 profiles ~~are separated by about~~ have separations of 2.~~5~~6° latitude ~~on the descending orbit.~~, and the solid curve (at 31.8°N) is closest to White Sands (WS, 32.4°N). Horizontal bars are ~~estimates of~~ ozone ~~error~~errors. (bottom) NH V6 ozone ~~distribution~~ at 4.6 hPa; Greenwich (0°E) is at right, and ~~contour interval (CI)~~CI is 0.5 ppmv. ~~Latitudes~~Latitude (dotted circles) ~~are spaced~~is every 10°. ~~The~~Satellite location is white dot (6°N, 265°E), and WS is blue dot ~~denotes White Sands~~.

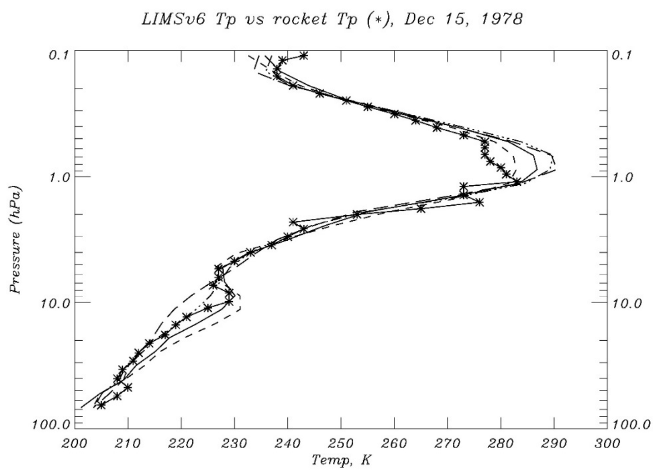

LIMSv6 Tp vs rocket Tp (*), Dec 15, 1978
Pressure (hPa)
0.1
1.0
10.0
100.0
200
210
220
230
240
250
260
270
280
290
300
Temp, K

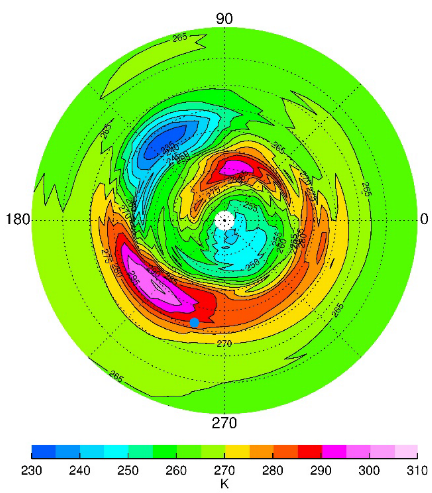

90
180
0
270
230
240
250
260
270
280
290
300
310
K

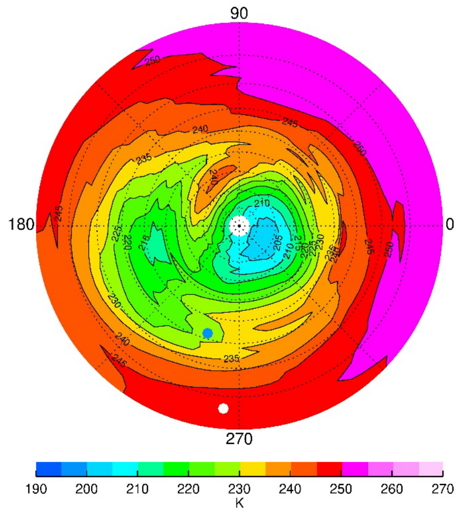

Figure 5—(top) Profiles of V6 temperature compared with Datasonde values (*) on December 15. The four V6 profiles are separated as in Fig. 4, where the short-dashed curve is for 29.2° and the long-dashed curve is for 37.2°. (bottom) NH V6 temperature distribution at ~~0.68~~4.6 hPa; ~~contour interval~~CI is 5 K, and ~~blue~~satellite location is white dot ~~denotes~~and White Sands is blue dot.

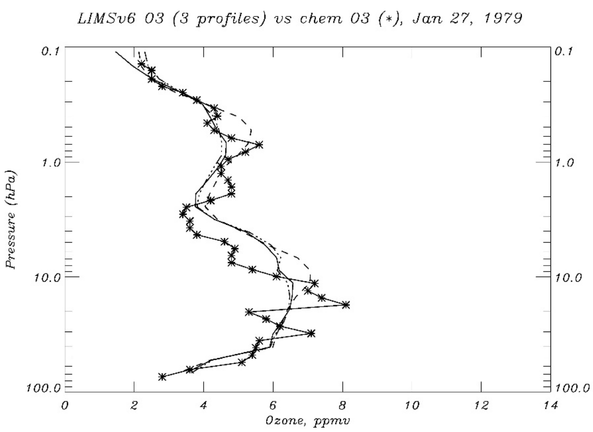
LIMSv6 O3 (3 profiles) vs chem O3 (*), Jan 27, 1979
Pressure (hPa)
0.1
1.0
10.0
100.0
0
2
4
6
8
10
12
14
Ozone, ppmv

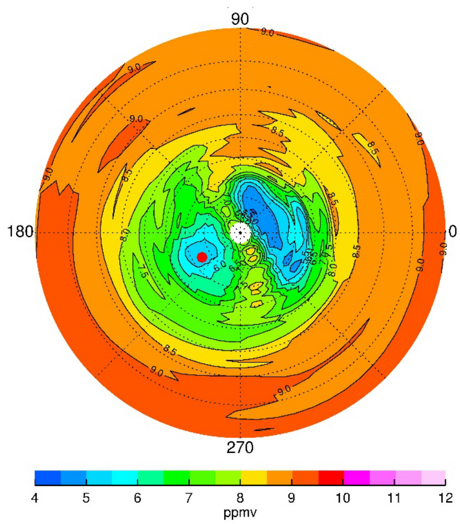
90
180
0
270
4
5
6
7
8
9
10
11
12
ppmv

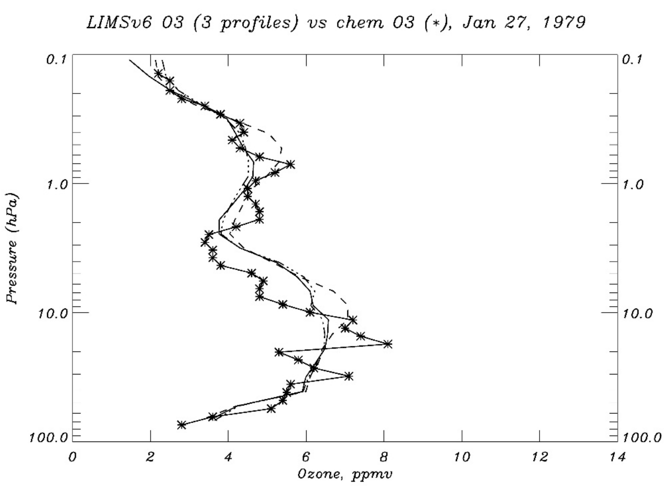
LIMSv6 O3 (3 profiles) vs chem O3 (*), Jan 27, 1979
Pressure (hPa)
0.1
1.0
10.0
100.0
0
2
4
6
8
10
12
14
Ozone, ppmv

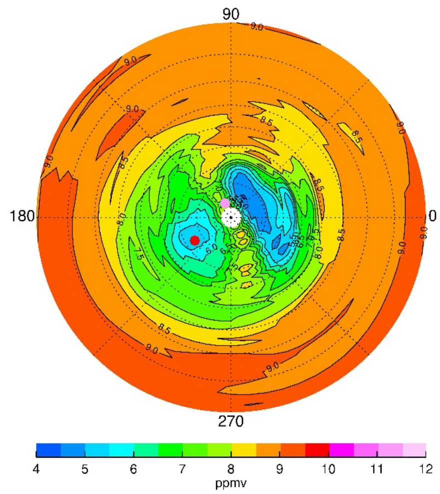

Figure 6—(top) As in Fig. 4, but for January 27, 1979, at Poker Flat, AK (65°N, 212.5°E); (bottom) NH V6 distribution of ozone at 4.6 hPa~~;~~, where CI is 0.5 ppmv ~~and red dot is~~ . Latitudes (dotted circles) are spaced every 10°; Poker Flat is red and satellite position (81°N, 113°E) is pink.

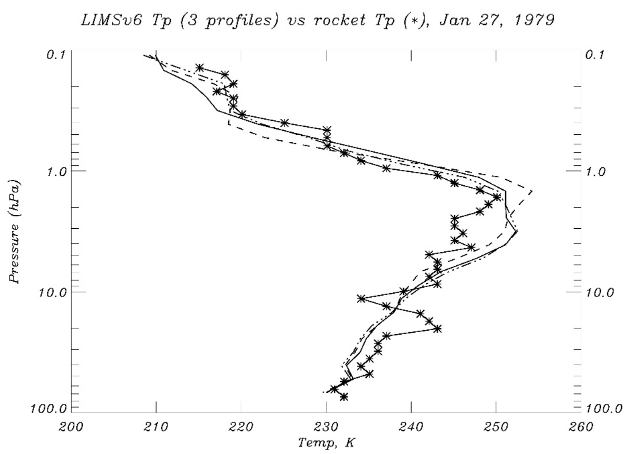
LIMSv6 Tp (3 profiles) vs rocket Tp (*), Jan 27, 1979
Pressure (hPa)
0.1
1.0
10.0
100.0
200
210
220
230
240
250
260
Temp, K

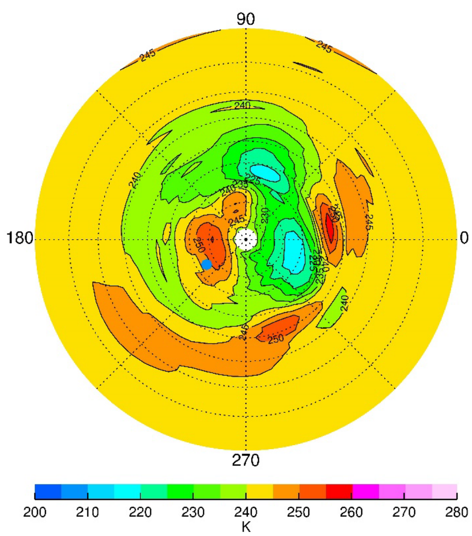
90
180
0
270
245
240
250
200
210
220
230
240
250
260
270
280
K

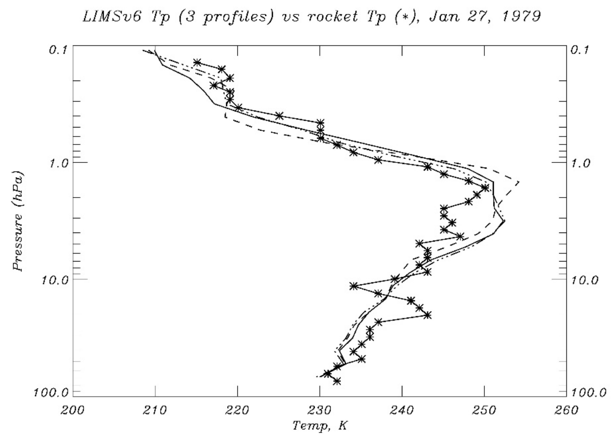

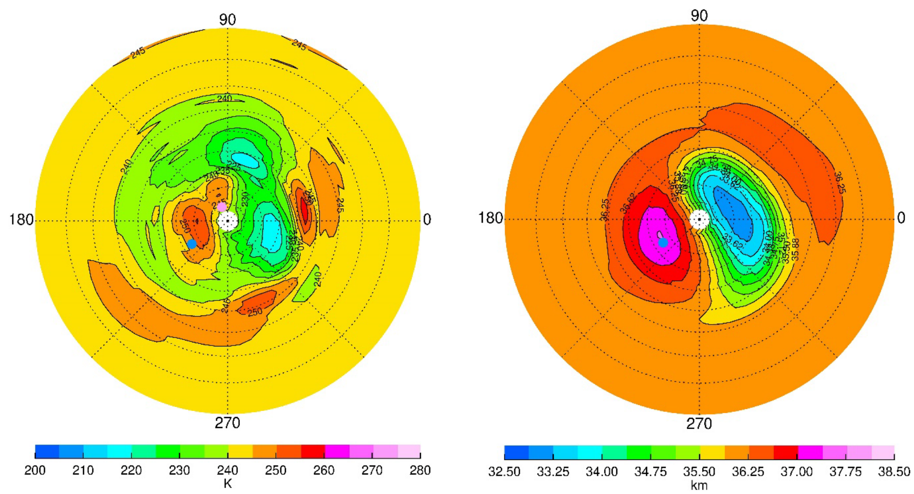

Figure 7—(top) As in Fig. 5, but for January 27, 1979. (bottom~~-~~left) NH V6 temperature~~ at 4.6 hPa on January 27; Contour interval~~; CI is 5 K. ~~Blue dot is location of ~~Poker Flat~~.~~

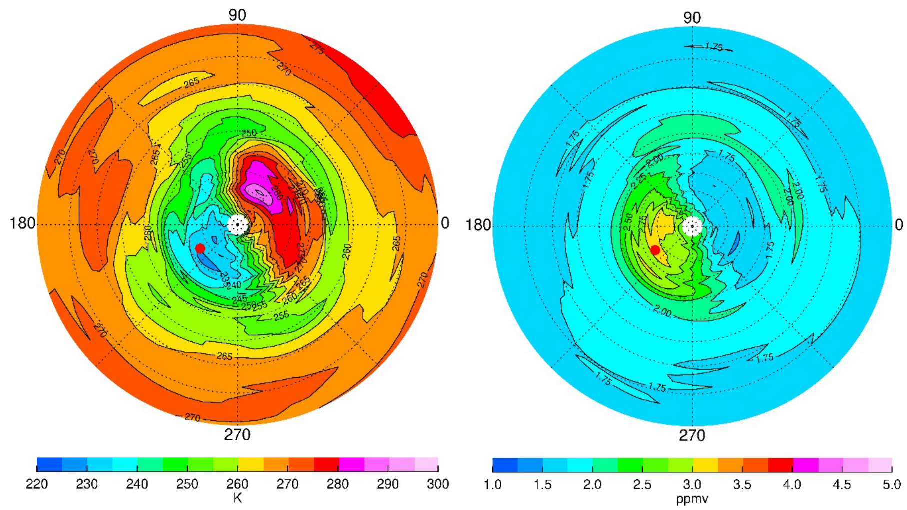

Figure 8 – (left) Temperature at 0.46 hPa for January 27, 1979, for comparison with is blueFig. 7. (right) Ozone at 0.46 hPa for comparison with Fig. 6. Contour interval for T(p) is 5 K and for ozone is 0.25 ppmv. Red dot is location of Poker Flat.

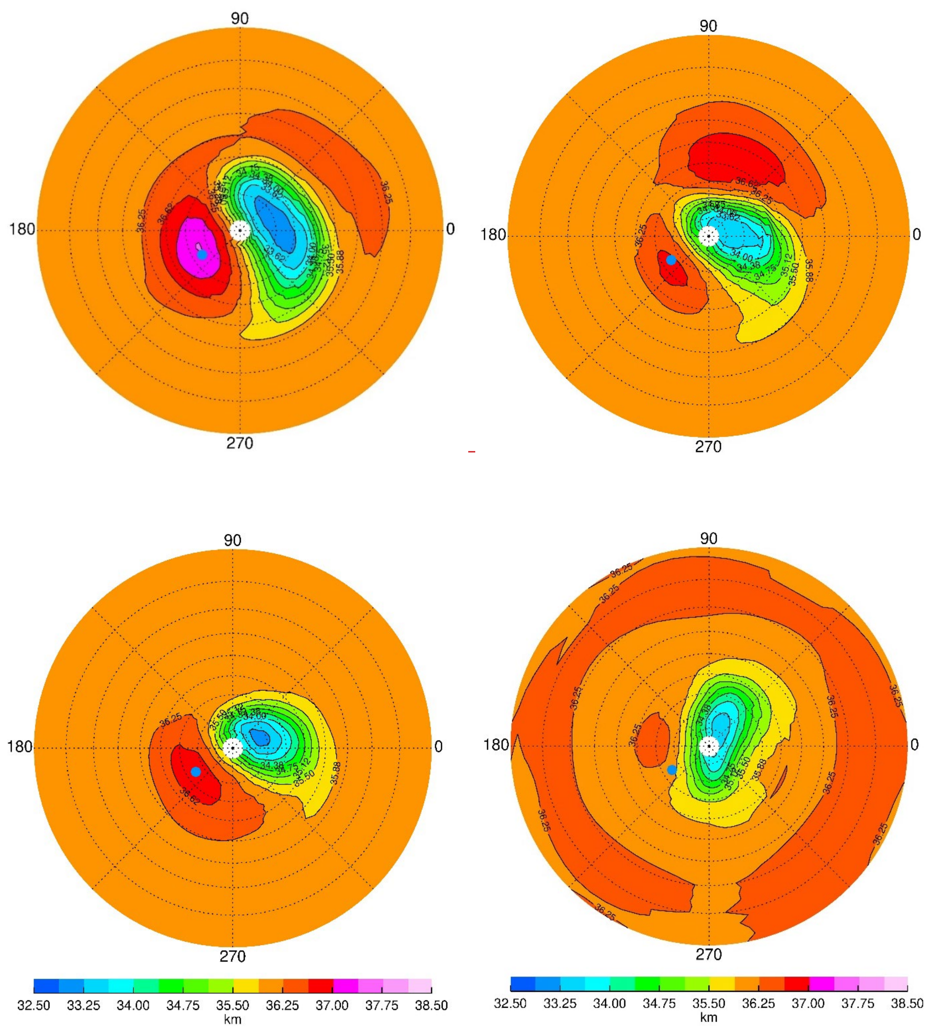

satellite position is pink. (bottom-right)

Figure 9 – NH V6 GPH at 4.6 hPa; contour interval (; CI) is 0.375 gpkm.

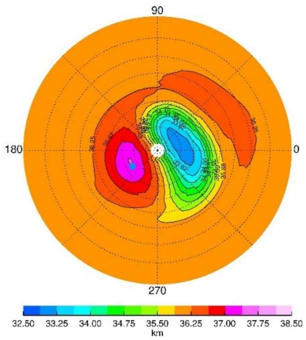

Figure Blue dot8—NH V6 GPH at 4.6 hPa; CI is location of0.375 gpkm. Poker Flat is blue dot. Panels are spaced one week apart; (top left) January 27; (top right) February 3; (bottom leftmiddle) February 10; and (bottom right) February 17.

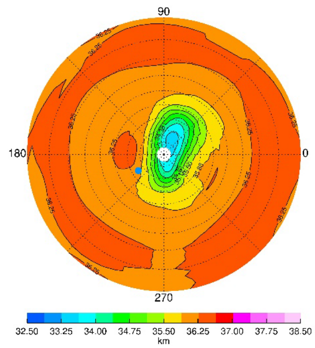

Formatted: Space After: 0 pt

Formatted: Font: Bold

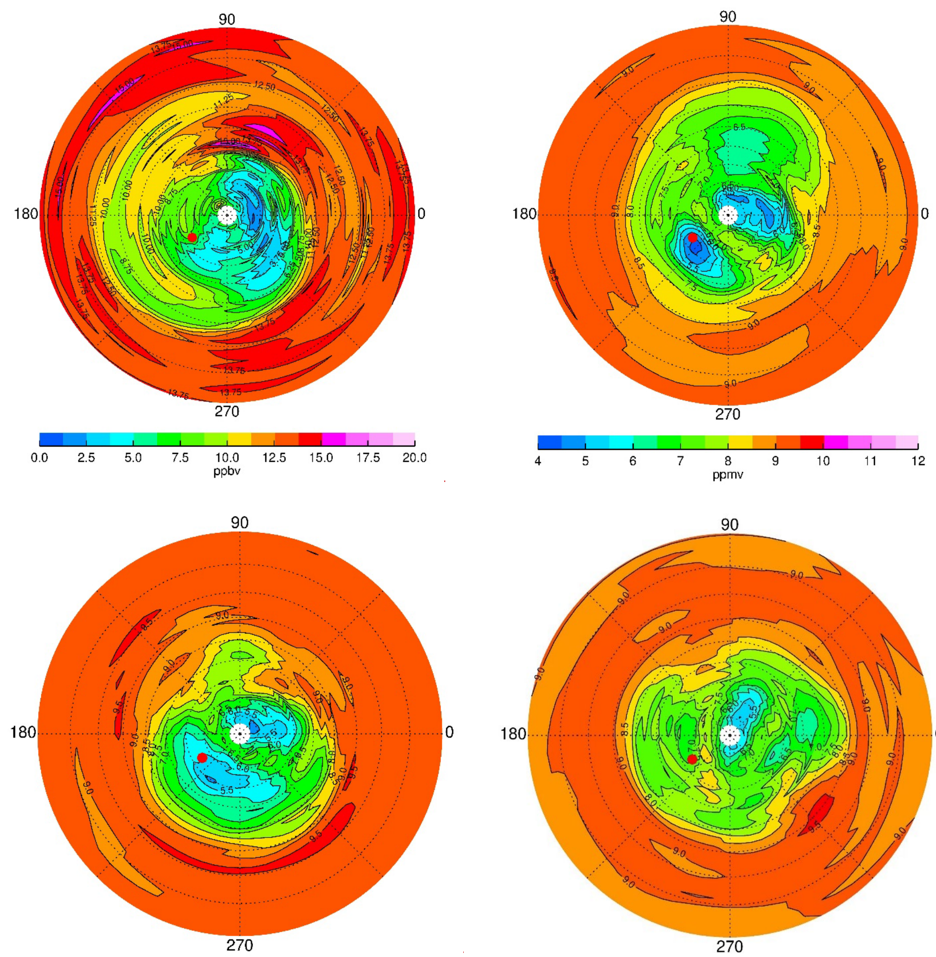
90
180
0
270
0.0 2.5 5.0 7.5 10.0 12.5 15.0 17.5 20.0
ppbv
4 5 6 7 8 9 10 11 12
ppmv

708

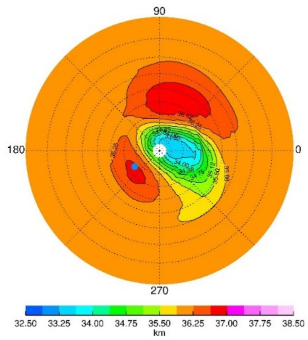

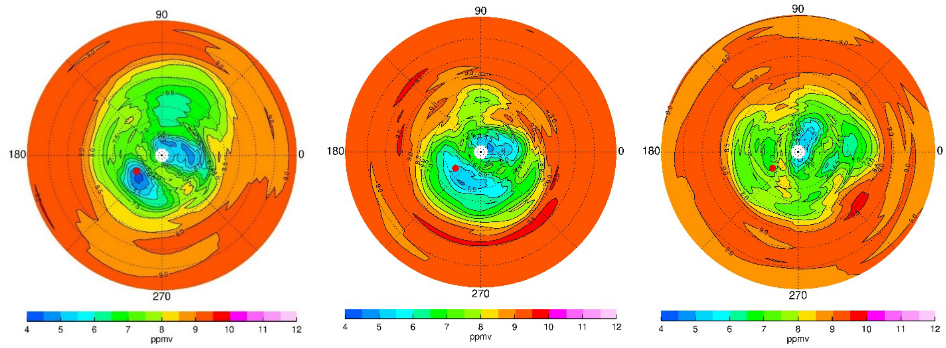

Figure ~~10~~9—Maps ~~for 4.6 hPa of (top left) nighttime NO_2 on January 27, CI is 1.25 ppbv and red dot is Poker Flat; (top right) ozone~~ of ozone at 4.6 hPa (left) on February 3~~; (bottom left) ozone~~, (middle) on February 10; and (~~bottom~~ right) ~~ozone~~ on February 17~~;~~. CI is 0.5 ppmv and red dot is Poker Flat.

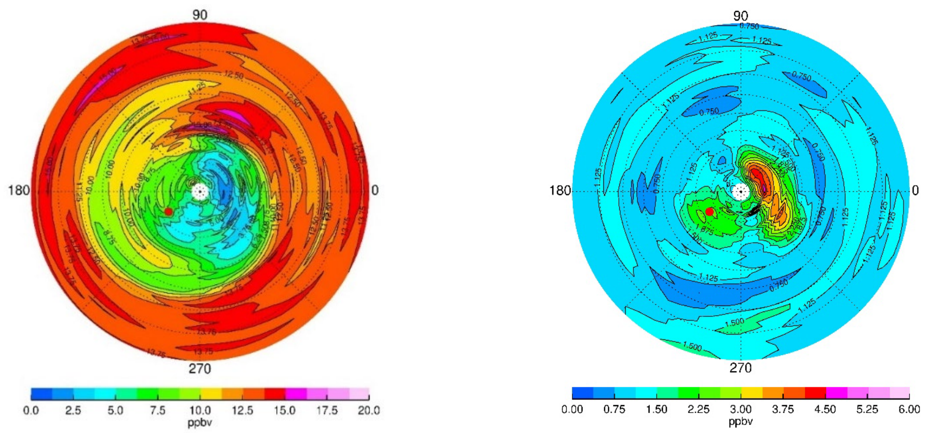

Figure 10—(left) Nighttime NO_2 on January 27 at 4.6 hPa; CI is 1.25 ppbv. (right) HNO_3 at 4.6 hPa; CI is 0.~~5 ppmv. Ozone color bar applies to the bottom two panels, as well~~375 ppbv. Red dot is Poker Flat.

Formatted: Space After: 0 pt

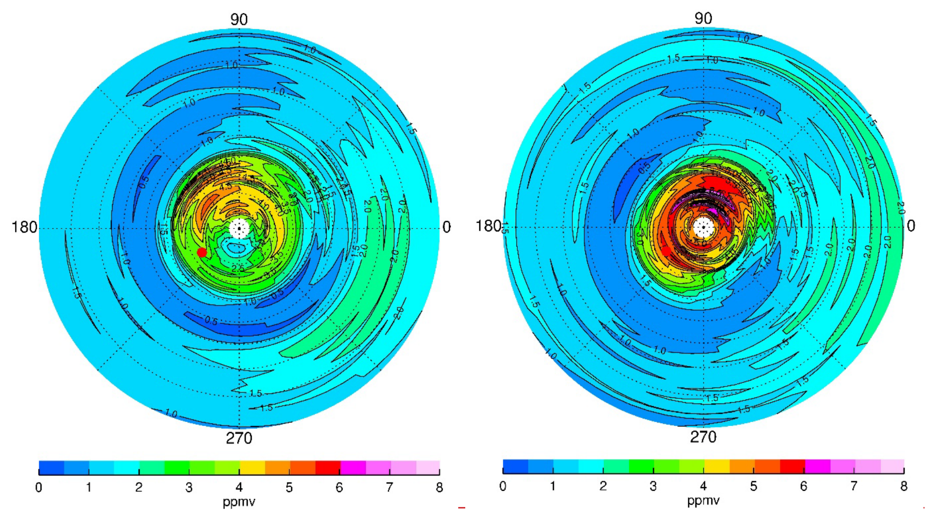

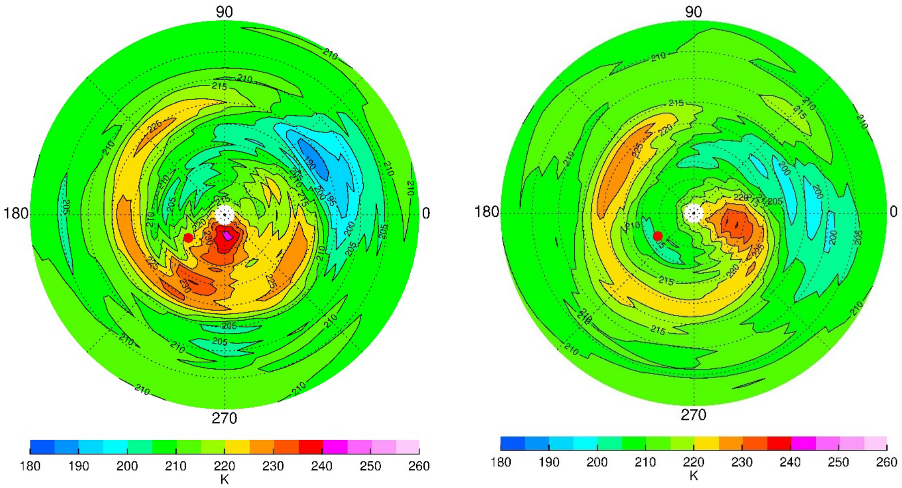
90
180
0
270
180 190 200 210 220 230 240 250 260
K
90
180
0
270
180 190 200 210 220 230 240 250 260
K

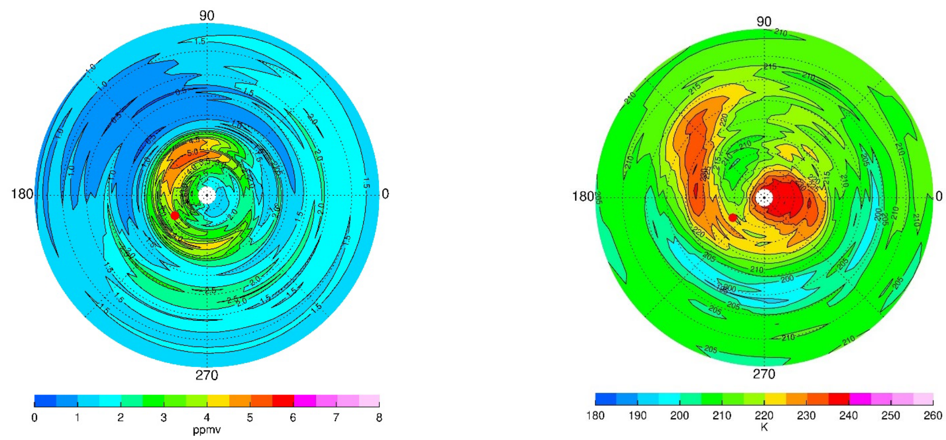

Figure 11—(top) ~~Distributions of~~ NH ~~ozone~~ distributions for December 15 at 0.022 hPa ~~on January 13~~for (left) ozone and ~~February 10 (right), respectively; contour interval is 0.5 ppmv. (bottom) NH~~ for (right) temperature ~~at 0.022 hPa on January 13 (left)~~; CIs are 0.5 ppmv and ~~February 10 (right); contour interval is 5 K.~~ 5 K, respectively. Red dot denotes location of Poker Flat.

Formatted: Space After: 0 pt

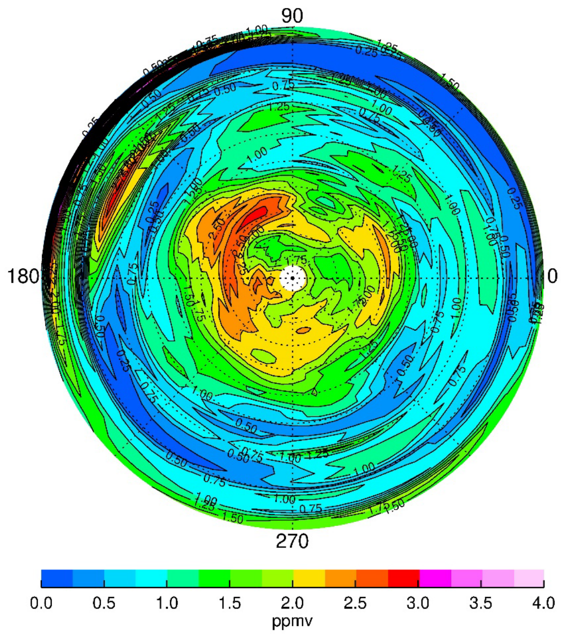
90
180
0
270
0.0
0.5
1.0
1.5
2.0
2.5
3.0
3.5
4.0
ppmv

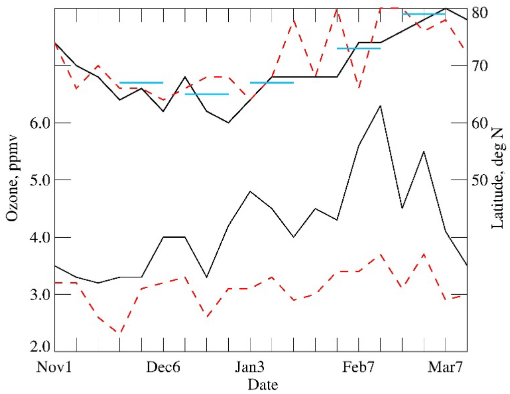

Figure 12—Time series of peak V6 ozone (bottom two curves) and its latitude location (top two curves) at 0.022 hPa. Dashed red curves are for combined ozone, while solid curves are for descending (nighttime) ozone only. Horizontal blue lines indicate the latitude of the terminator.

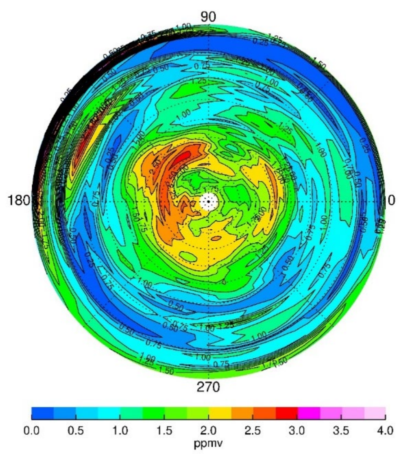

Figure 13—NH V6 combined (A+D) ozone distribution at 68 hPa for December 15, 1978. ~~Contour interval~~CI is 0.25 ppmv.

References

Andrews, D. G., Holton, J. R., and Leovy, C. B.: *Middle Atmosphere Dynamics*, 1st Ed., 489 pp., Academic Press, 1987.

Chandran, A., Collins, R. L., Garcia, R. R., Marsh, D. L., Harvey, V. L., Yue, J., and de la Torre, L.: A climatology of elevated stratopause events in the whole atmosphere community climate model, J. Geophys. Res. Atmos., 118, 1234-1246, https://doi.org/10.1002/jgrd.50123, 2013.

de la Cámara, A., Abalos, M., Hitchcock, P., Calvo, N., and Garcia, R. R.: Response of Arctic ozone to sudden stratospheric warmings, Atmos. Chem. Phys., 18, 16499–16513, https://doi.org/10.5194/acp-18-16499-2018, 2018.

Edwards, D. P., Kumer, J. B., Lopez-Puertas, M., Mlynczak, M. G., Gopalan, A., Gille, J. C., and Roche, A.: Non-local thermodynamic equilibrium limb radiance near 10 µm as measured by UARS CLAES, J. Geophys. Res., 101, D21, 26,577-26,588, https://doi.org/10.1029/96JD02133, 1996.

Fleming, E.L., Chandra, S., Barnett, J. J., and Corney, M.: Zonal mean temperature, pressure, zonal wind, and geopotential height as functions of latitude, COSPAR International Reference Atmosphere: 1986, Part II: Middle Atmosphere Models, Adv. Space Res., 10 (12), 11-59, https://doi.org/10.1016/0273-1177(90)90386-E, 1990.

Funke, B., López-Puertas, M., Garcia-Comas, M., Kaufmann, M., Höpfner, M., and Stiller, G. P.: GRANADA: a generic RAdiative traNsfer AnD non-LTE population algorithm, J. Quant. Spectros. Radiat. Transfer, 113, 1771–1817, https://doi.org/doi: 10.1016/j.jqsrt.2012.05.001, 2012.

Gettelman, A., Hoor, P., Pan, L. L., Randel, W. J., Hegglin, M. I., and Birner, T.: The extratropical upper troposphere and lower stratosphere, Rev. Geophys., 49, RG3033, https://doi.org/10.1029/2011RG000355, 2011.

Gille, J. C. and Russell III, J. M.: The limb infrared monitor of the stratosphere: experiment description, performance, and results, J. Geophys. Res., 84, 5125-5140, https://doi.org/10.1029/JD089iD04p05125, 1984.

Harvey, V. L., Pierce, R. B., Hitchman, M. H., Randall, C. E., and Fairlie, T. D.: On the distribution of ozone in stratospheric anticyclones, J. Geophys. Res., 109, D24308, https://doi:10.1029/2004JD004992, 2004.

Harvey, V. L., Randall, C. E., Manney, G. L., and Singleton, C. S.: Low-ozone pockets observed by EOS-MLS, J. Geophys. Res., 113, D17112, https://doi.org/10.1029/2007JD009181, 2008.

Hegglin, M. I., Tegtmeier, S., Anderson, J., Bourassa, A. E., Brohede, S., Degenstein, D., Froidevaux, L., Funke, B., Gille, J., Kasai, Y., Kyrola, E. T., Lumpe, J., Murtagh, D., Neu, J. L., Perot, K., Remsberg, E. E., Rozanov, A., Toohey, M., Urban, J., von Clarmann, T., Walker, K. A., Wang, H-J.., Arosio, C., Damadeo, R., Fuller, R. A., Lingenfelser, G., McLinden, C., Pendelbury, D., Roth, C., Ryan, N. J., Sioris, C., Smith, L., and Weigel, K.: Overview and update of the SPARC Data Initiative: comparison of stratospheric composition measurements from satellite limb sounders, Earth Syst. Sci. Data, 13, 1855-1903, https://doi.org/10.5194/essd-1855-2021, 2021.

Hilsenrath, E.: Rocket observations of the vertical distribution of ozone in the polar night and during a mid-winter stratospheric warming, Geophys. Res. Lett., 7, 581-584, https://doi.org/10.1029/GL007i008p00581, 1980.

Hilsenrath, E., and Kirschner, P. T.: Recent assessment of the performance and accuracy of a chemiluminescent rocket sonde for upper atmospheric ozone measurements, Rev. Sci. Instrum., Vol. 51, 1381-1389, https://doi.org/10.1063/1.1136080, 1980.

Hitchman, M. H., Gille, J. C., Rodgers, C. D., and Brasseur, G.: The separated polar winter stratopause: a wave driven climatological feature, J. Atmos. Sci., 46, 410-422, https://doi.org/10.1175/1520-0469(1989)046%3C0410:TSPWSA%3E2.0.CO;2, 1989.

Holt, L. A., Randall, C. E., Harvey, V. L., Remsberg, E. E., Stiller, G. P., Funke, B., Bernath, P. F., and Walker, K. A., Atmospheric effects of energetic particle precipitation in the Arctic winter 1978–1979 revisited, J. Geophys. Res., 117, D05315, https://doi.org/10.1029/2011JD016663, 2012.

Kim, J-H., Jee, G., Choi, H., Kim, B-M., and Kim, S-J.: Vertical structures of temperature and ozone changes in the stratosphere and mesosphere during stratospheric sudden warmings, J. Astron. Space Sci., 37, 69-75, https://doi.org/10.5140/JASS.2020.37.1.69, 2020.

Leovy, C. B., Sun, C-R., Hitchman, M. H., Remsberg, E. E., Russell, III, J. M., Gordley, L. L., Gille, J. C., and Lyjak, L. V.: Transport of ozone in the middle stratosphere: evidence for planetary wave breaking, J. Atmos. Sci., 42, 230-244, https://doi.org/10.1175/1520-0469(1985)042%3C0230:TOOITM%3E2.0.CO;2, 1985.

Lieberman, R. S., Oberheide, J., Hagan, M. E., Remsberg, E. E., and Gordley, L. L.: Variability of diurnal tides and planetary waves during November 1978–May 1979, J. Atmos. Solar-Terr. Phys., 66, 517–528, https://doi.org/10.1016/j.jastp.2004.01.006, 2004.

Lopez-Puertas, M. and Taylor, F. W.: Non-LTE Radiative transfer in the Atmosphere, World Scientific Publ. Co., River Edge, NJ, USA, 504 pp., 2001.

López-Puertas, M., García-Comas, M., Funke, B., Gardini, A., Stiller, G. P., Clarmann, T. von, Glatthor, N., Laeng, A., Kaufmann, M., Sofieva, V. F., Froidevaux, L., Walker, K. A., and Shiotani, M.: MIPAS observations of ozone in the middle atmosphere, Atmos. Meas. Tech., 11, 2187–2212, https://doi.org/10.5194/amt-11-2187-2018, 2018.

Manney, G. L., Froidevaux, L., Waters, J. W., Zurek, R. W., Gille, J. C., Kumer, J. B., Mergenthaler, J. L., Roche, A. E., O'Neill, A., and Swinbank, R.: Formation of low-ozone pockets in the middle stratospheric anticyclone during winter, J. Geophys. Res. Atmos., 100, 13939-13950, https://doi.org/10.1029/95JD00372, 1995.

Marsh, D., Smith, A., Brasseur, G., Kaufmann, M., and Grossmann, K.: The existence of a tertiary ozone maximum in the high-latitude middle mesosphere, Geophys. Res. Lett., 28, 4531-4534, https://doi.org/10.1029/2001GL013791, 2001.

Manuilova, R. O., Gusev, O. A., Kutepov, A. A., von Clarmann, T., Oelhaf, H., Stiller, G. P, Wegner, A., Lopez-Puertas, M., Martin-Torres, F. J., Zaragoza, G., and Flaud, J.-M.: Modelling of non-LTE limb spectra of i.r. ozone bands for the MIPAS space experiment, J. Quant. Spectrosc. Rad. Transf., 59, 405-422, https://doi.org/10.1016/S0022-4073(97)00120-9, 1998.

Mlynczak, M. G. and Drayson, R.: Calculation of infrared limb emission by ozone in the terrestrial middle atmosphere 2. Emission calculations, J. Geophys. Res., 95, 16,513-16,521, https://doi.org/10.1029/JD095iD10p16513, 1990.

Morris, G. A., Kawa, S. R., Douglass, A. R., Schoeberl, M. R., Froidevaux, L., and Waters, J., Low-ozone pockets explained, J. Geophys. Res., 103, 3599-3610, https://doi.org/10.1029/97JD02513, 1998.

Nair, H., Allen, M., Froidevaux, L., and Zurek, R.: Localized rapid ozone loss in the northern winter stratosphere: An analysis of UARS observations, J. Geophys. Res., 103, 1555-1571, **https://doi.org/10.1029/97JD03072**, 1998.

Remsberg, E., and Lingenfelser, G.: LIMS Version 6 Level 3 dataset, NASA-TM-2010-216690, available at http://www.sti.nasa.gov (last access: 17 September 2019), 13 pp., 2010.

Remsberg, E. E., Haggard, K. V., and Russell III, J. M~~.,~~.: Estimation of synoptic fields of middle atmosphere parameters from Nimbus-7 LIMS profile data, J. Atmos. Ocean. Tech, 7, 689-705, https://doi.org/10.1175/1520-0426(1990)007%3C0689:EOSFOM%3E2.0.CO;2, 1990.

Remsberg, E. E., Gordley, L. L, Marshall, B. T., Thompson, R. E., Burton, J., Bhatt, P., Harvey, V. L., Lingenfelser, G., Natarajan, M.: The Nimbus 7 LIMS version 6 radiance conditioning and temperature retrieval methods and results, J. Quant. Spectros. Rad. Transf., 86, 395-424, doi:10.1016/j.jqsrt.2003.12.007, 2004.

Remsberg, E., Lingenfelser, G., Natarajan, M., Gordley, L., Marshall, B. T., and Thompson, E.: On the quality of the Nimbus 7 LIMS version 6 ozone for studies of the middle atmosphere, J. Quant. Spectros. Rad. Transf., 105, 492-518, doi:10.1016/j.jqsrt.2006.12.005, 2007.

Remsberg, E., ~~et al~~Lingenfelser, G., and Natarajan, M.: LIMS/Nimbus-7 Level 3 Daily 2 deg Latitude Zonal Fourier Coefficients of O3, NO2, H2O, HNO3, Geopotential Height, and Temperature V006, Version: 006, Goddard Earth Sciences Data and Information Services Center

(GES DISC), available at: https://disc.gsfc.nasa.gov/datacollection/LIMSN7L3_006.html (last access: 11 March 2021), 2011.

Remsberg, E., Natarajan, M., Fairlie, T. D., Wargan, K., Pawson, S., Coy, L., Lingenfelser, G., and Kim, G.: On the inclusion of Limb Infrared Monitor of the Stratosphere version 6 ozone in a data assimilation system, J. Geophys. Res., 118, 7982-8000, https://doi.org/10.1002/jgrd.50566, 2013.

Remsberg, E., Natarajan, M., and Harvey, V. L.: On the consistency of HNO_3 and NO_2 in the Aleutian High region from the Nimbus 7 LIMS Version 6 dataset, Atmos. Meas. Tech., 11, 3611-3626, https://doi.org/10.5194/amt-11-3611-2018, 2018.

Remsberg, E., Harvey, V. L., Krueger, A., and Natarajan, M.: Residual temperature bias effects in stratospheric species distributions from LIMS, Atmos. Meas. Tech., 14, 2185-2199, https://doi.org/10.5194/amt-14-2185-2021,https://doi.org/10.5194/amt-14-2185-2021, 2021.

Shams, S. B., von Walden, P., Hannigan, J. W., Randel, W. J., Petropavlovskikh, I. V., Butler, A. H., and de la Cámara, A.: Analyzing ozone variations and uncertainties at high latitudes during sudden stratospheric warming events using MERRA-2, Atmos. Chem. Phys. Disc., https://doi.org/10.5194/acp-2021-646, 2021.

Shepherd, T. G., Plummer, D. A., Scinocca, J. F., Hegglin, M. I., Fioletov, V. E., Reader, M. C., Remsberg, E., von Clarmann, T., and Wang, H. J.: Reconciliation of halogen-induced ozone loss with the total-column record, Nature Geoscience, 7, 443-449, doi:10.1038/ngeo2155, 2014.

Formatted: Space After: Auto

Siskind, D. E., Coy, L., Espy, P.: Observations of stratospheric warmings and mesospheric coolings by the TIMED SABER instrument, Geophys. Res. Lett. 32, http://doi.org/10.1029/2005GL022399, 2005.

Siskind, D. E., Harvey, V. L., Sassi, F., McCormack, J. P., Randall, C. E., Hervig, M. E., and Bailey, S. M.: Two- and three-dimensional structures of the descent of mesospheric trace constituents after the 2013 sudden stratospheric warming elevated stratopause event, Atmos. Chem. Phys., 21, 14059–14077, https://doi.org/10.5194/acp-21-14059-2021, 2021.

Smith, A. K., López-Puertas, M., García-Comas, M., and Tukiainen, S.: SABER observations of mesospheric ozone during NH late winter 2002–2009, Geophys. Res. Lett., 36, L23804, https://doi.org/10.1029/2009GL040942, 2009.

Smith, A. K., Garcia, R. R., Marsh, D. R., and Richter, J. A.: WACCM simulations of the mean circulation and trace species transport in the winter mesosphere, J. Geophys. Res., 116, D20115, **https://doi.org/10.1029/2011JD016083**, 2011.

Smith, A. K., Espy, P. J., López-Puertas, M., and Tweedy, O. V., Spatial and temporal structure of the tertiary ozone maximum in the polar winter mesosphere, J. Geophys. Res., 123, 4373-4389, https://doi.org/10.1029/2017JD028030, 2018.

Sofieva, V. F., Szeląg M., Tamminen, J., Kyrölä, E., Degenstein, D., Roth, C., Zawada, D., Rozanov, A., Arosio, C., Burrows, J. P., Weber, M., Laeng, A., Stiller, G. P., von Clarmann, T., Froidevaux, L., Livesey, N., van Roozendael, M., and Retscher, C.: Measurement report: regional trends of stratospheric ozone evaluated using the MErged GRIdded Dataset of Ozone Profiles (MEGRIDOP), Atmos. Chem. Phys., 21, 6707–6720, https://doi.org/10.5194/acp-21-6707-2021, 2021.

Solomon, S., Kiehl, J. T., Kerridge, B. J., Remsberg, E. E., and Russell III, J. M.: Evidence for nonlocal thermodynamic equilibrium in the ν_3 mode of mesospheric ozone, J. Geophys. Res., 91, 9865-9876, https://doi.org/10.1029/JD091iD09p09865, 1986.

SPARC, Assessment of Stratospheric Aerosol Properties, L. Thomason and Th. Peter, Ed., WCRP-124, WMO/TD- No. 1295, SPARC Report No. 4, 322 pp., 2006.

SPARC: The SPARC Data Initiative: Assessment of stratospheric trace gas and aerosol climatologies from satellite limb sounders, Hegglin, M. I. and Tegtmeier, S., (Eds.), SPARC Report No. 8, WCRP-5/2017, http://www.sparc-climate.org/publications/sparc-reports/, 2017.

Stolarski, R. S., Douglass, A. R., Remsberg, E. E., Livesey, N. J., and Gille, J. C.: Ozone temperature correlations in the upper stratosphere as a measure of chlorine content, J. Geophys. Res., 117, D10305, https://doi.org/10.1029/2012JD017456. 2012.

Tegtmeier, S., Hegglin, M. I., Anderson, J., Bourassa, A., Brohede, S., Degenstein, D., Froidevaux, L., Fuller, R., Funke, B., Gille, J., Jones, A., Kasai, Y., Krüger, K., Kyrölä, E., Lingenfelser, G., Lumpe, J., Nardi, B., Neu, J., Pendlebury, D., Remsberg, E., Rozanov, A., Smith, L., Toohey, M., Urban, J., von Clarmann, T., Walker, K. A. and Wang, R. H. H.: SPARC Data Initiative: A comparison of ozone climatologies from international satellite limb sounders, J. Geophys. Res., 118, 12,229-12,247, https://doi.org/10.1002/2013JD019877, 2013.

WOUDC, World Ozone and Ultraviolet Radiation Data Centre, ~~https://woudc.org/home.php.~~https://woudc.org/home.php.